ISSN 1674-1056
http://cpb.iphy.ac.cn
http://iopscience.iop.org/cpb
中国物理 B
Chinese Physics
中国物理 Chinese Physics B

Damage and recovery of fiber Bragg grating under radiation environment

Shi-Zhe Wen(温世喆)[1,6], Wei-Chen Xiong(熊伟晨)[3,6], Li-Ping Huang(黄力平)[4,6], Zhen-Rui Wang(王镇锐)[4,6], Xing-Bin Zhang(张兴斌)[5,6], Zhen-Hui He(何振辉)[2,5,6]

Citation: Chin. Phys. B . 2018, 27(9): 090701. **doi:** 10.1088/1674-1056/27/9/090701

Journal homepage: http://cpb.iphy.ac.cn; http://iopscience.iop.org/cpb

What follows is a list of articles you may be interested in

Damage and recovery of fiber Bragg grating under radiation environment

Shi-Zhe Wen(温世喆)[1,6], Wei-Chen Xiong(熊伟晨)[3,6], Li-Ping Huang(黄力平)[4,6], Zhen-Rui Wang(王镇锐)[4,6], Xing-Bin Zhang(张兴斌)[5,6], Zhen-Hui He(何振辉)[2,5,6]

Chin. Phys. B . 2018, 27(9): 090701. **doi:** 10.1088/1674-1056/27/9/090701

Highly-sensitive NO, NO_2, and NH_3 measurements with an open-multipass cell based on mid-infrared wavelength modulation spectroscopy

Xiang Chen(陈祥), Chen-Guang Yang(杨晨光), Mai Hu(胡迈), Jian-Kang Shen(沈建康), Er-Chao Niu(牛二超), Zhen-Yu Xu(许振宇), Xue-Li Fan(范雪丽), Min Wei(魏敏), Lu Yao(姚路), Ya-Bai He(何亚柏), Jian-Guo Liu(刘建国), Rui-Feng Kan(阚瑞峰)

Chin. Phys. B . 2018, 27(4): 040701. **doi:** 10.1088/1674-1056/27/4/040701

Optical sensors based on the NiPc–CoPc composite films deposited by drop casting and under the action of centrifugal force

Noshin Fatima, Muhammad M Ahmed, Khasan S Karimov, Zubair Ahmad, Fahmi Fariq Muhammad

Chin. Phys. B . 2017, 26(6): 060704. **doi:** 10.1088/1674-1056/26/6/060704

Room temperature NO_2-sensing properties of hexagonal tungsten oxide nanorods

Yaqiao Wu(武雅乔), Ming Hu(胡明), Yuming Tian(田玉明)

Chin. Phys. B . 2017, 26(2): 020701. **doi:** 10.1088/1674-1056/26/2/020701

Effect of bias condition on heavy ion radiation in bipolar junction transistor

Liu Chao-Ming, Li Xing-Ji, Geng Hong-Bin, Yang De-Zhuang, He Shi-Yu

Chin. Phys. B . 2012, 21(8): 080703. **doi:** 10.1088/1674-1056/21/8/080703

Damage and recovery of fiber Bragg grating under radiation environment*

Shi-Zhe Wen(温世喆)[1,6], Wei-Chen Xiong(熊伟晨)[3,6], Li-Ping Huang(黄力平)[4,6], Zhen-Rui Wang(王镇锐)[4,6], Xing-Bin Zhang(张兴斌)[5,6], and Zhen-Hui He(何振辉)[2,5,6,†]

[1] School of Material Science and Engineering, Sun Yat-Sen University, Guangzhou 510006, China
[2] State Key Laboratory of Optoelectronic Materials and Technologies, Sun Yat-Sen University, Guangzhou 510275, China
[3] School of Engineering, Sun Yat-Sen University, Guangzhou 510006, China
[4] School of Physics, Sun Yat-Sen University, Guangzhou 510275, China
[5] School of Physics and Astronomy, Sun Yat-Sen University, Zhuhai 519000, China
[6] Center for Space Technology, Sun-Yat Sen University, Zhuhai 519000, China

(Received 5 March 2018; revised manuscript received 23 April 2018; published online 10 August 2018)

To develop the application of fiber Bragg gratings as temperature and strain sensors in space environments, it is necessary to understand the effect of high-energy radiation on the performance of the fiber Bragg grating. We performed an experiment involving Co^{60}-γ ionizing irradiation with a total dose of 1.01×10^6 rad on two Ge-doped single-mode fiber Bragg gratings with central wavelengths of 825 and 835 nm, respectively. We found that, with the increase of radiation dose, the redshift of the peak wavelength of the reflection spectrum of the fiber Bragg gratings indicated the increase of the refractive index and the number of color centers. After irradiation, the refractive index decreased with the decreasing number of color centers. We analyzed the influence of ionizing irradiation on the transmission performance of the fiber Bragg gratings using a color-center model, which explained the experimental results. The proposed model was used to determine the creation rate and annihilation rates of the color center, which are foundational data for using the fiber Bragg gratings in space applications.

Keywords: fiber Bragg grating, radiation, color center, refractive index, damage, recovery, annihilation

PACS: 07.07.Df, 07.60.Vg, 42.81.Cn **DOI:** 10.1088/1674-1056/27/9/090701

1. Introduction

Fiber Bragg gratings are regarded as filters or mirrors for lasers with the corresponding wavelength. Through internal writing and ultraviolet phase mask exposure, the refractive index of a grating exhibits a periodic distribution. With the above features, Bragg gratings can be used as optical devices, having the advantages of small size, lightness, high strength, anti-electromagnetic interference, corrosion resistance, easy coupling with fibers, small coupling loss, and low cost. In satellite laser communications, fiber Bragg gratings can be used as a narrow-band filter, for wavelength-division multiplexing (WDM) and as a demultiplexing unit of WDM systems, and as an optical branching multiplexer.[1–3] Additionally, fiber-optic sensors can detect the working status of satellites or nuclear facilities through the displacement, speed, temperature, and other measurements of the reaction of the facilities to ensure their operating health.[4–6] Fiber Bragg gratings have better multiplexing performance and can be used for sensing and transferring data, whereby it is easy to form a sensor network.[7]

To evaluate the performance of fiber Bragg gratings in high-energy radiation environments, e.g., in space or nuclear facilities, experiments should be performed in similar environments to understand the effect of the radiation on the grating performance. Because of high cost, long period, and difficulty, a Co60-γ source is typically used to simulate the radiation environment. Ferdinand[4] and Gusarov[5,6] conducted γ and neutron radiation experiments on a fiber Bragg grating on a germanium fiber and observed the increase of the peak wavelength and the refractive index of the light reflected from the grating. The phenomenon was attributed to the color centers created by ionizing radiation. Finally, they did not conduct an in-depth analysis of the regularity and tendency of the color centers.[4–6]

A common feature of aerospace and nuclear reactors is the harsh radiation environment, which can damage the performance of fiber-optic components.[1,4–6,8,9] Radiation is deposited on the material mainly in two ways: the displacement of atoms and ionization. Owing to the strong covalent-bond structure in silica optical fiber, it is very difficult for radiation particles to displace the atoms. Therefore, the ionization effect is the major cause of defects.[10] For silica fiber, the ionization effect shifts an electron to the neighboring atoms and thus creates a defect called a color centers. The created color centers

*Project supported by the Project for the State Key Laboratory of Optoelectronic Materials and Technologies of China (Grant No. 09010-32031708) and the Project for Zhuhai Key Laboratory of Center for Space Technology of China (Grant No. 71000-42080001).

†Corresponding author. E-mail: stshzh@mail.sysu.edu.cn

© 2018 Chinese Physical Society and IOP Publishing Ltd

change the optical absorption spectrum,[11–15] modifying the refractive index of the fiber Bragg grating.[1,6,16]

In recent years, among several studies investigating the space radiation effects on optical fibers,[17–19] few paid attention to the radiation damage to fiber Bragg gratings, and none investigated the recovery from such damage.

In this study, to examine the radiation effects on the fiber Bragg grating, an experiment involving γ^{60}Co irradiation, along with post-irradiation annealing at room temperature, was performed. According to the model for the creation and annihilation of color centers, the creation rate and the annihilation rate of color centers were fitted from the experiment data, and the shift of the central wavelength caused by the irradiation was predicted and set as the systematic error.

2. Radiation-created color-center model

Ma *et al.*[16] introduced a model of color-center creation and degradation, where the created color centers can be degraded back to the intrinsic defects by the radiation, and the degradation rate of the color center is proportional to the radiation rate. However, this assumption was not supported by their experimental results, which indicated that the properties of the fiber recovered gradually after radiation, indicating that the color-center concentration decreased when there was no radiation.

We consider a different model of color-center creation and annihilation. Color centers can be created by high-energy radiation but are unstable and can be annihilated by thermal annealing. That is, under constant irradiation over a long period of time, the creation rate becomes equal to the annihilation rate, and the color-center concentration becomes constant. Consider the combined effect of the color-center creation rate $k_{\rm c}$, which is proportional to the radiation dose rate $R_{\rm d}$ and to the concentration of atoms in regions without color center N_0, as well as the color-center annihilation rate $k_{\rm a}$, which is proportional to the available concentration of color center $n(t)$. The variation of the color-center concentration in the fiber can be expressed as

$$\frac{{\rm d}n(t)}{{\rm d}t} = -k_{\rm a}n(t) + k_{\rm c}[N_0 - n(t)], \tag{1}$$

$$k_{\rm c} = R_{\rm d}\kappa_{\rm c}, \tag{2}$$

where $\kappa_{\rm c}$ is a coefficient of the dose rate, and t is the irradiation time. $k_{\rm c}$ and $k_{\rm a}$ can be obtained by fitting the measured data.

When $k_{\rm c} \neq 0$, the solution of equation (1) gives

$$n(t) = \frac{\kappa_{\rm c}R_{\rm d}N}{\kappa_{\rm c}R_{\rm d}+k_{\rm a}}\left(1 - {\rm e}^{-(\kappa_{\rm c}R_{\rm d}t+k_{\rm a}t)}\right). \tag{3}$$

By replacing $R_{\rm d}t$ in Eq. (3) with the irradiation dose $D = R_{\rm d}t$, equation (3) can be rewritten as

$$n(t) = \frac{k_{\rm c}N}{k_{\rm c}+k_{\rm a}}\left(1 - {\rm e}^{-(\kappa_{\rm c}D+k_{\rm a}t)}\right). \tag{4}$$

When irradiation is stopped, $k_{\rm c} = 0$, and equation (1) becomes

$$\frac{{\rm d}n(t)}{{\rm d}t} = -k_{\rm a}n(t) \tag{5}$$

with the solution

$$n(t) = n(t_0)\,{\rm e}^{-k_{\rm a}(t-t_0)}, \tag{6}$$

where $n(t_0)$ is the color-center concentration immediately after the irradiation is stopped.

$$n(t_0) = \frac{\kappa_{\rm c}R_{\rm d}N}{\kappa_{\rm c}R_{\rm d}+k_{\rm a}}\left(1 - {\rm e}^{-(\kappa_{\rm c}R_{\rm d}t_0+k_{\rm a}t_0)}\right). \tag{7}$$

In Smakula's equation,[20] the absorption coefficient is proportional to the color-center concentration

$$\alpha \propto n_i(t). \tag{8}$$

According to the Kramers–Kroning causality law,[21] the relation between the absorption coefficient and the refractive index can be expressed as

$$\Delta n_z = \frac{1}{4\pi\sqrt{\pi \ln 2}}\sum_i \frac{\Delta\alpha_{\rm max}\Delta\lambda_{1/2}}{1-(\lambda_i/\lambda')^2}, \tag{9}$$

where λ_i is the center wavelength of the i-th absorption band, $\Delta\alpha_{\rm max}$ is the variation of the peak absorption, $\Delta\lambda_{1/2}$ is the full width at half maximum (FWHM) of the absorption band, and λ' is the wavelength of interest.

Consider the simplest case: for an optical fiber Bragg grating around 800 nm, the ionizing effect of electron radiation on the grating mainly produces one type of color center,[22] which leads to an absorption spectrum of Gaussian approximation. When the FWHM of the absorption band is a certain value, from Eqs. (4), (8), and (9), we obtain the following relationship for the fiber Bragg grating under irradiation:

$$\Delta n_z = \eta\frac{\kappa_{\rm c}R_{\rm d}N}{\kappa_{\rm c}R_{\rm d}+k_{\rm a}}\left(1 - {\rm e}^{-(\kappa_{\rm c}R_{\rm d}t+k_{\rm a}t)}\right), \quad R_{\rm d} \neq 0, \tag{10}$$

$$\Delta n_z = \varphi\,{\rm e}^{-k_{\rm a}(t-t_0)}, \quad R_{\rm d} = 0, \tag{11}$$

where η is a constant associated with the type of color center and the absorption spectrum, and φ is a constant associated with the initial color-center concentration and η.

From the Bragg grating equation

$$\lambda_{\rm max} \approx \lambda_{\rm B} = 2n_z\Lambda, \tag{12}$$

we have

$$\Delta n_z = \frac{\Delta\lambda_{\rm max}}{2\Lambda}, \tag{13}$$

where $\Delta\lambda_{\rm max}$ is the peak wavelength variation, Λ is the grating period length, and $\lambda_{\rm B}$ is the Bragg wavelength.

After radiation, Δn_z can be obtained from the measured $\Delta\lambda_{\rm max}$, and then η can be obtained by fitting Eq. (10). Finally, the effect of high-energy radiation on the fiber Bragg grating sensor can be predicted.

3. Experiments

3.1. Apparatus and method

The fiber Bragg gratings used in this experiment were procured from FBGS. The gratings were inscribed on a germanium-doped (10%–20%) single-mode fiber via the phase mask method. The fiber core diameter and cladding diameter were 4.5 and 125 μm, respectively, and the coating material was modified organic ceramics, with the temperature sensitivity of the Bragg wavelength of the grating being 5.5 pm/°C (according to the data sheet for the fiber Bragg grating). The parameters of the grating sample are shown in Table 1, and the grating structure under the microscope is shown in Fig. 1.

Table 1. Parameters of optical fiber Bragg gratings.

Number	Peak wavelength/nm	Fiber type
Fiber 1	824.979	SMF
Fiber 2	834.978	SMF

Notes: "SMF" means "single-mode fiber"

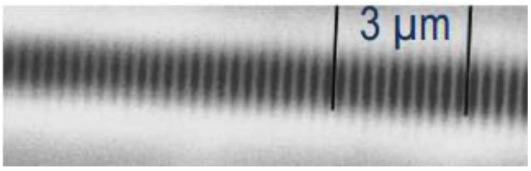


Fig. 1. (color online) Fiber Bragg grating structure.

The radiation source used in the experiment was the ^{60}Co-γ radiation source from Guangzhou Huada Biological Co., Ltd. The grating section of the optical fiber was exposed in a ^{60}Co-γ-ray radiation chamber, while the other part of the optical fiber was protected by a 3-mm-thick lead tube. Near the grating section, a low-range potassium dichromate dosimeter was used to measure the radiation dose. The irradiation period of 2 h for each data point was not strictly controlled, with an uncertainty of 10 min. After each irradiation, the reflection spectrum of the fiber sample was measured. The interval between two irradiations was hours on the same day, or overnight, depending on the working time of the company. The total radiation dose was 1.01×10^6 rad. A K-type thermocouple was used to monitor the ambient temperature.

A sketch of the experimental setup is shown in Fig. 2. The built-in wavelength of the light source ranges from 800 to 860 nm, and the intensity is approximately 0.3 mW. The emitted light passes through the fiber optic splitter and then is split into two beams of equal intensity to the two fiber Bragg grating. The two specific wavelengths of light are reflected into the spectrometer. Through an array of charge-coupled devices (CCDs), the reflected light intensity at its wavelength is transformed into an electrical signal to record the reflection spectrum.

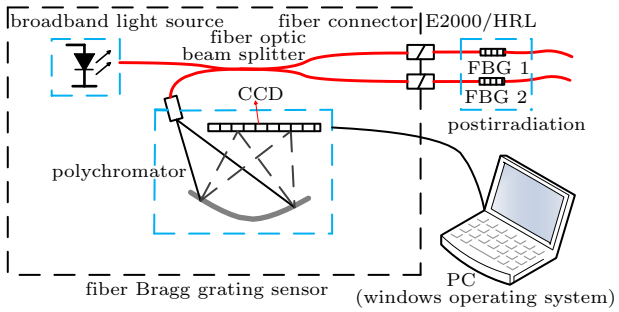


Fig. 2. (color online) Experimental setup for the radiation experiments of fiber Bragg gratings.

3.2. Radiation dose error analysis

The main sources of measurement uncertainty are the magnitude of the change of the light absorption before and after irradiation, ΔA, and the ambient temperature T. The sum of squared uncertainties is multiplied by the dose response conversion factor $K\,(=8.33)$ to obtain the total uncertainty of the measurement. The K-type thermocouple temperature measurement accuracy is ±0.5 K, and the absorbance accuracy A is 0.001; the dose uncertainty can be calculated using the following equation:

$$D = K\Delta A\,[1+0.0015(T-20)]\,. \tag{14}$$

The relative error of the calculated dose is

$$\begin{aligned}\frac{\delta_D}{D} &= \frac{\left|\frac{\partial D}{\partial T}\delta_T\right|+\left|\frac{\partial D}{\partial A_0}\delta_{A_0}\right|+\left|\frac{\partial D}{\partial A_\mathrm{f}}\delta_{A_\mathrm{f}}\right|}{D}\\ &= \frac{|0.0015K\Delta A\delta_T|+|K\delta_{A_0}|+|K\delta_{A_\mathrm{f}}|}{D}.\end{aligned} \tag{15}$$

Table 2 shows the absorbed dose errors at different dose rates. The relative error varies from 0.39% to 0.77%.

Table 2. Absorbed dose error.

Number	Light absorbance before radiation A_0	Light absorbance after radiation A_f	Average temperature/°C	Absorbed dose/kGy	Absolute error/kGy	Relative error/%
1	0.957	0.717	20.0	2.0	±0.0086	±0.43
2	0.965	0.701	20.0	2.2	±0.0087	±0.39
3	0.957	0.753	19.1	1.7	±0.0086	±0.50
4	0.957	0.753	19.2	1.7	±0.0086	±0.50
5	0.966	0.834	18.9	1.1	±0.0085	±0.77
6	0.954	0.786	19.1	1.4	±0.0085	±0.61

4. Results and discussion

4.1. Effect of radiation dose on reflection spectrum

Tables 3 and 4 show the variation of the peak refractive wavelengths of the 825- and 835-nm fiber Bragg gratings, respectively, according to the radiation dose. As the temperature of the fiber Bragg grating changes by 1.0 °C, the peak wavelength changes by 5.5 pm. Considering the effect of the ambient temperature, the peak wavelengths of the fiber Bragg gratings were corrected. Figures 3 and 4 show the reflection spectrum in two grating samples before and after irradiation, where a redshift of the peak wavelength is obviously observed. The 825- and 835-nm peak wavelengths increase by 0.0706 and 0.0742 nm, respectively. The FWHM of the reflected wave does not change significantly with the increase of the irradiation dose (see Tables 5 and 6). With the increase of the irradiation dose, the intensity of the reflected wave of Bragg grating first increases and then decreases (see Tables 5 and 6), indicating that the light-transmission characteristics of the fiber were impaired by the radiation.

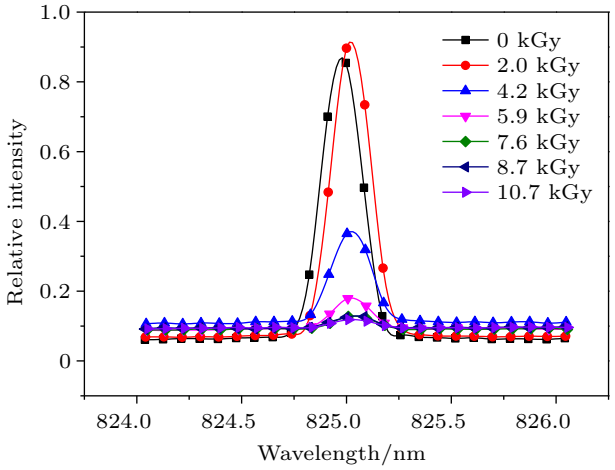


Fig. 3. (color online) Reflective spectrum variation of the 825-nm optical Bragg grating pre-radiation and post-radiation.

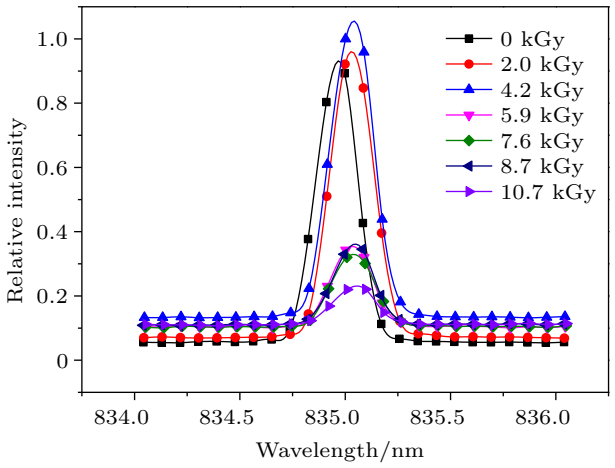


Fig. 4. (color online) Reflective spectrum variation of the 835-nm optical fiber pre-radiation and post-radiation.

Table 3. 825-nm Bragg grating wavelength variation with respect to radiation dose.

Dose/kGy	Bragg wavelength/nm	Temperature/°C	Corrected wavelength (20 °C)/nm
0	824.988	21.9	824.979
2.0	824.984	19.0	824.989
4.2	825.021	18.9	825.026
5.9	825.031	19.0	825.036
7.6	825.033	18.8	825.039
8.7	825.040	19.0	825.045
10.1	825.045	19.2	825.049

Table 4. 835-nm Bragg grating wavelength variation with respect to radiation dose.

Dose/kGy	Bragg wavelength/nm	Temperature/°C	Corrected wavelength (20 °C)/nm
0	834.987	21.8	834.978
2.0	834.988	19.0	834.993
4.2	835.022	18.9	835.027
5.9	835.039	19.0	835.044
7.6	835.040	18.8	835.046
8.7	835.041	19.0	835.046
10.1	835.048	19.2	835.052

Table 5. 825-nm Bragg grating FWHM and relative intensity variation with respect to radiation dose.

Dose/kGy	FWHM/nm	Relative intensity
0	0.214	0.887
2.0	0.209	0.930
4.2	0.212	0.376
5.9	0.203	0.181
7.6	0.208	0.129
8.7	0.208	0.130
10.1	0.211	0.120

Table 6. 835-nm Bragg grating FWHM and relative intensity variation with respect to radiation dose.

Dose/kGy	FWHM/nm	Relative intensity
0	0.220	0.943
2.0	0.229	0.977
4.2	0.229	1.075
5.9	0.222	0.359
7.6	0.231	0.334
8.7	0.216	0.364
10.1	0.225	0.230

4.2. Effect of radiation dose on refractive index of fiber Bragg grating

According to the experimental results, the difference between the peak wavelength of fiber Bragg grating before and after radiation could be obtained at different radiation doses.

The measurement accuracy of the peak wavelength of the Bragg grating reflection was 0.1 pm. Because the ambient temperature influenced the peak wavelength of the reflection, in the data-processing operation, the peak wavelength was converted into the corresponding wavelength at 20 °C. The

thermocouple temperature measurement accuracy was 0.5 K. The conversion equation is

$$\frac{T-20}{0.02(^{\circ}\mathrm{C})}=\frac{\lambda-\lambda_{\max}}{0.0001(\mathrm{nm})}, \tag{16}$$

or

$$\lambda_{\max}=\lambda-\frac{T-20}{200}, \tag{17}$$

where $\lambda_{\max}$ is the peak wavelength corresponding to the ambient temperature of 20 °C, λ is the peak wavelength actually measured, and T is the ambient temperature. Therefore, the uncertainty of $\lambda_{\max}$ is

$$\delta_{\lambda_{\max}}=\pm\left(|\delta_{\lambda}|+\left|\frac{\delta_T}{200}\right|\right). \tag{18}$$

From Eq. (9), the uncertainty of the refractive-index variation is

$$\delta_{\Delta n}=\pm\left|\frac{\delta_{\lambda_{\max}}}{2\Lambda}\right|. \tag{19}$$

The variation of the refractive index of the fiber Bragg grating at different doses is shown in Tables 7 and 8. The refractive index varies exponentially with time, in agreement with Eq. (10).

Table 7. 825-nm Bragg grating refractive-index variation with respect to radiation dose.

Time/min	Dose/kGy	Refractive index variation (20 °C)/10^{-5}	Absolute error/10^{-5}	Relative error/%
143	2.0	1.293	0.303	23.43
300	4.2	5.710	0.303	5.31
421	5.9	6.977	0.303	4.34
543	7.6	7.281	0.303	4.16
621	8.7	8.044	0.303	3.77
721	10.1	8.560	0.303	3.54

Table 8. 835-nm Bragg grating refractive-index variation with respect to radiation dose.

Time/min	Dose/kGy	Refractive index variation (20 °C)/10^{-5}	Absolute error/10^{-5}	Relative error/%
143	2.0	1.885	0.311	16.50
300	4.2	5.932	0.311	5.24
421	5.9	7.898	0.311	3.94
543	7.6	8.145	0.311	3.82
621	8.7	8.151	0.311	3.82
721	10.1	8.880	0.311	3.50

4.3. Color-center annihilation

After radiation ($R_{\mathrm{d}}=0$ at this time), the peak wavelength of the grating reflection had a recovery or annealing effect (color-center annihilation); thus, k_{a} can be obtained by fitting the recovery-effect curve. Then, we can obtain the particular parameters in Eq. (7) with the annealing results.

After ionizing radiation at 1.0×10^{6} rad, the two fiber Bragg gratings were placed at room temperature, and their refractive-index variation with time was measured. The experimental results are shown in Tables 9 and 10 and Fig. 5. The refractive index of both fibers gradually decreases with time.

Table 9. 825-nm Bragg grating recovery effect.

Time/day	Bragg wavelength/nm	Temperature/°C	Corrected wavelength (20 °C)/nm	Corrected refractive index variation (10^{-5})
3	825.053	23.5	825.036	6.920
4	825.046	23.8	825.027	5.897
5	825.038	22.7	825.024	5.513
6	825.042	24.0	825.022	5.247
8	825.042	23.9	825.022	5.293
9	825.038	23.7	825.019	4.932
10	825.041	24.2	825.020	4.954
11	825.037	24.1	825.016	4.532
12	825.038	24.3	825.017	4.622

Table 10. 835-nm Bragg grating recovery effect.

Time/day	Bragg wavelength/nm	Temperature/°C	Corrected wavelength (20 °C)/nm	Corrected refractive index variation (10^{-5})
3	835.064	23.5	835.046	8.184
4	835.052	23.8	835.033	6.587
5	835.044	22.7	835.030	6.280
6	835.048	24.0	835.028	6.005
8	835.045	23.9	835.025	5.672
9	835.045	23.7	835.027	5.869
10	835.043	24.2	835.022	5.346
11	835.041	24.1	835.020	5.087
12	835.043	24.3	835.022	5.254

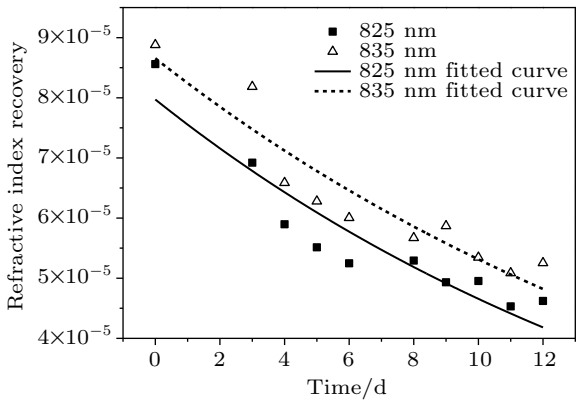


Fig. 5. (color online) Refractive-index recovery with time, after radiation. The black squares and triangles represent the measured refractive-index data for 825 and 835 nm, respectively. The black line and dashed line are the curves fitted with the color-center annihilation model for 825 and 835 nm, respectively.

The color center created by the radiation is unstable and will gradually be annihilated. According to Eq. (11) and the experimental data presented in Tables 9 and 10, the fitted equations for the fiber Bragg gratings with Bragg wavelengths of 825 and 835 nm are $y=8.0\times10^{-5}\,\mathrm{e}^{-0.054t}$ and $y=8.7\times10^{-5}\,\mathrm{e}^{-0.049t}$, respectively, where t represents time (see Fig. 5). Therefore, we obtain $k_{\mathrm{a_825}}=0.054/24/60\ \mathrm{min}=3.8\times10^{-5}\ \mathrm{min}^{-1}$ and $k_{\mathrm{a_835}}=0.049/24/60\ \mathrm{min}=3.4\times10^{-5}\ \mathrm{min}^{-1}$, respectively.

To evaluate the reliability of the recovery curves, the error of the fitted curve and the experimental data points were determined.

$$X_i = \Delta n_{zi} - y_i, \tag{20}$$

$$\sigma^2 = \frac{1}{10}\sum_{i=1}^{10}(X_i - \bar{X})^2, \tag{21}$$

where X_i is the deviation of the measured data from the fitted value y_i, and σ is the standard deviation of X_i. σ is 4.18×10^{-6} and 4.22×10^{-6} for 825-nm and 835-nm gratings, respectively. Therefore, k_{a_825} and k_{a_835} with random error are expressed as follows:

$$k_{a_825} = 3.8\pm0.5\times10^{-5}\ \text{min}^{-1}, \tag{22}$$

$$k_{a_835} = 3.4\pm0.5\times10^{-5}\ \text{min}^{-1}. \tag{23}$$

From Fig. 6, the deviations of the fitted data are within 3σ. According to the 3σ criterion, the fitted curve is reliable.

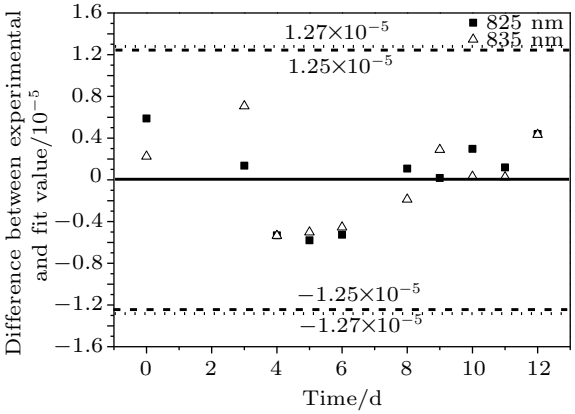


Fig. 6. (color online) 3σ judgment for the difference of the experimental data points from the fitted values. The black squares and triangles represent the difference between the measured refractive-index variances and the fitted recovery curve for 825-nm and 835-nm gratings, respectively. They are within the region of 3σ judgment between the black dotted lines and dashed lines for 825 and 835 nm, respectively.

4.4. Refractive-index variation with correction

According to the color-center annihilation mechanism, the refractive index recovers in each irradiation interval. Therefore, the refractive-index variations were corrected according to the fitted annihilation rate. Owing to the time interval between the placement in the irradiation chamber and the start time of the measurement, the correction time of the grating has an uncertainty of 10 min, which yields a refractive-index variation of 3.0×10^{-8}. Tables 11 and 12 show the time interval and corrected refractive-index variation time. The fitted curves are shown in Fig. 7.

According to k_a from the annealing experiment and the fitted curve in Fig. 7, the relationship between the variations of the effective refractive index of the optical fiber with 825- and 835-nm Bragg gratings and their absorbed dose are as follows:

$$\Delta n_{825\ \text{nm}} = 1.3\times10^{-4}\left(1-\text{e}^{-1.9\times10^{-3}t}\right), \tag{24}$$

$$\Delta n_{835\ \text{nm}} = 1.1\times10^{-4}\left(1-\text{e}^{-2.4\times10^{-3}t}\right). \tag{25}$$

From Eqs. (10) and (22)–(25), $k_{a_825}+\kappa_{c_825}R_d = 1.9\times10^{-3}$, and $k_{a_835}+\kappa_{c_835}R_d = 2.4\times10^{-3}$. As R_d = 1400 rad/min, $k_{a_825} = 3.8\times10^{-5}$ min^{-1}, $k_{a_835} = 3.4\times10^{-5}$ min^{-1}, $\kappa_{c_825} = 1.3\times10^{-6}$, and $\kappa_{c_835} = 1.7\times10^{-6}$.

The relationships between the refractive-index variation for Bragg wavelengths of 825 and 835 nm and the radiation time and dose rate are as follows:

$$\Delta n_{z_825\ \text{nm}} = \frac{1.7\times10^{-4}R_d}{38+1.3R_d}\left(1-\text{e}^{-3.8\times10^{-5}t-1.3\times10^{-6}R_dt}\right), \tag{26}$$

$$\Delta n_{z_835\ \text{nm}} = \frac{1.9\times10^{-4}R_d}{34+1.7R_d}\left(1-\text{e}^{-3.4\times10^{-5}t-1.7\times10^{-6}R_dt}\right). \tag{27}$$

Table 11. Corrected 825-nm Bragg grating refractive-index variation with respect to radiation dose.

Time/min	Refractive index variation (20 °C)/10^{-5}	Time interval/min	Refraction index recovery during interval/10^{-6}	Corrected refractive index variation/10^{-5}
143	1.293	0	0	1.293
300	5.710	720	8.009	6.511
421	6.977	240	6.600	7.637
543	7.281	1020	8.877	8.169
621	8.044	150	6.333	8.677
721	8.560	120	6.244	9.184

Table 12. Corrected 835-nm Bragg grating refractive-index variation with radiation dose.

Time/min	Refractive index variation (20 °C)/10^{-5}	Time interval/min	Refraction index recovery during interval/10^{-6}	Corrected refractive index variation/10^{-5}
143	2.0	0	0	1.885
300	4.2	720	1.102	6.366
421	5.9	240	9.736	8.193
543	7.6	1020	1.181	8.665
621	8.7	150	9.494	8.420
721	10.1	120	9.413	9.140

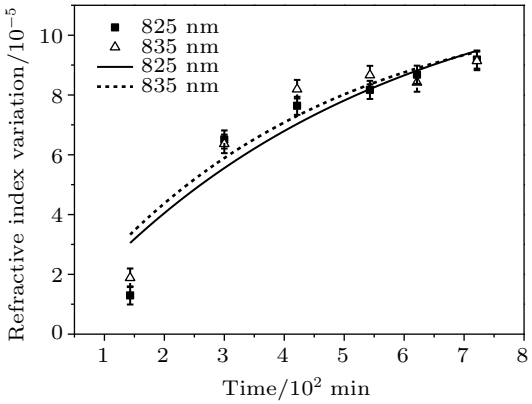


Fig. 7. (color online) Refractive-index variation with respect to the radiation time after recovery correction. The black squares and triangles represent the refractive-index data with respect to time (different doses) for 825- and 825-nm gratings, respectively. The black line and dashed line are the curves fitted using the color-center creation model for 825 and 835 nm, respectively.

4.5. Prediction of space radiation effects on fiber Bragg grating

According to the refractive-index variation and damage recovery, the 825- and 835-nm fiber grating color-center creation rates were $k_{c_825} = \kappa c_825 R_d = 1.3 \times 10^{-6} R_d$ and $k_{c_835} = \kappa_{c_835} R_d = 1.7 \times 10^{-6} R_d$, respectively, and the annihilation rates were $k_{a_825} = 3.8 \times 10^{-5}$ min^{-1} and $k_{a_835} = 3.4 \times 10^{-5}$ min^{-1}, respectively. Therefore, the average color-center creation rate was

$$k_c = \frac{\kappa_{c_825} + \kappa_{c_835}}{2} R_d = 1.5 \times 10^{-6} R_d,$$

and the average color-center annihilation rate was

$$k_a = \frac{k_{a_825} + k_{a_835}}{2} = 3.6 \times 10^{-5}.$$

Combining Eqs. (26) and (27) by averaging the related parameters gives the variation of the refractive index of the fiber Bragg grating with respect to the radiation dose and time

$$\Delta n_z = \frac{1.8 \times 10^{-4} R_d}{36 + 1.5 R_d} \left(1 - e^{-3.6 \times 10^{-5} t - 1.5 \times 10^{-6} R_d t}\right). \quad (28)$$

With Eq. (28), the application performance of the fiber Bragg gratings in radiation environments can be predicted. For example, in the case of temperature measurement, the temperature drift caused by the radiation can be predicted in low Earth orbit and Earth synchronous orbit. For a wavelength variation of 5.5 pm/°C, according to Eq. (13), the temperature drift caused by radiation is

$$\Delta T = \frac{2\Lambda}{5.5 \times 10^{-3}} \Delta n_z. \quad (29)$$

In low Earth orbit, the dose rate is $R_{d1} = 1.2 \times \frac{10^4 \text{ rad}}{\text{year}} = 2.3 \times 10^{-2}$ rad/min, and the temperature drift due to radiation is

$$\Delta T_{\text{low_earth}} = 0.0182 \left(1 - e^{-3.6 \times 10^{-5} t}\right). \quad (30)$$

According to Eq. (30), in low Earth orbit, after 125 d (180,000 min), the maximum drift of the temperature measurement is 0.018 K, which can be regarded as systematic error. Such uncertainty caused by radiation can satisfy most of the requirements for the measurement accuracy in applications.

In Earth synchronous orbit, the dose rate is $R_{d2} = 5.2 \times 10^5$ rad/year $= 9.9 \times 10^{-1}$ rad/min. Then, the temperature drift due to radiation is

$$\Delta T_{\text{synch_earth}} = 0.712 \left(1 - e^{-3.6 \times 10^{-5} t}\right). \quad (31)$$

According to Eq. (31), in low Earth orbit, after 125 d (180,000 min), the maximum drift of the temperature measurement is 0.71 K.

5. Summary

We built a model of color-center creation by ionizing radiation with annihilation to study the shift and recovery of the refractive index of fiber Bragg gratings made of silica under and after ^{60}Co γ radiation. By fitting the experimental data of the refractive-index shift, we obtained the model parameters. The effect of the radiation on the performance of the silica fiber Bragg gratings can thus be quantitively predicted for applications, e.g., temperature measurement in low Earth orbit and Earth synchronous orbit. The deviation of the refractive index of the grating in a known radiation environment can be regarded as a systematic error. This makes it possible to apply the silica fiber Bragg gratings as sensors in high-energy radiation environments, e.g., in space and nuclear facilities. However, the model provides a mechanism for the creation and annihilation of color centers, which elucidates the effect of radiation on the silica fiber Bragg gratings.

References

[1] Gusarov A I, Doyle D B, Karafolas N and Berghmans F 2000 *Int. Symp. Opt. Sci. Technol.* P. 253
[2] Marshall P W, Dale C J and Burke E A 1992 *Nucl. Sci. IEEE Trans.* **39** 1982
[3] Ott M, Plante J, Shaw J, Shaw J, Garrisondarrin M, Ott M, Plante J and Garrisondarrin M 1997 *Aiaa Journal*
[4] Ferdin, P, Magne S, Marty V and Georges T 1994 *Proc. SPIE* **2425** 11
[5] Gusarov A, Fernandez A F, Vasiliev S, Medvedkov O, Blondel M and Berghmans F 2002 *Nucl. Instrum. & Methods Phys. Res.* **187** 79
[6] Gusarov A I, Berghmans F, Deparis O and Fernandez A F 1999 *Photon. Technol. Lett. IEEE* **11** 1159
[7] Marshall P W, Dale C J, Carts M A and Label K A 1994 *Nucl. Sci. IEEE Trans.* **41** 1958
[8] Girard S, Tortech B, Regnier E, Uffelen M V, Gusarov A, Ouerdane Y, Baggio J, Paillet P, Ferlet-Cavrois V and Boukenter A 2007 *IEEE Trans. Nucl. Sci.* **54** 2426
[9] Zhou C M, Zhang F, Ding L and Jiang D S 2011 *Laser & Optoelectronics Prog.* **48** 9
[10] Holmes Siedle A and Adams L 2001 (Oxford University Press)
[11] Jiang H, Chen B X, Fu C S, Sui G R and Ji S 2010 *Acta Phys. Sin.* **59** 7782 (in Chinese)
[12] Neustruev V B 1994 *J. Phys.: Condens. Matter* **6** 6901
[13] Regnier E, Flammer I, Girard S, Gooijer F, Achten F and Kuyt G 2007 *IEEE Trans. Nucl. Sci.* **54** 1115
[14] Russell P S, PoyntzWright L J and Hand D P 1991 *in: San Jose-DL tentative*
[15] Xiao Z Y, Luo W Y and Wang T Y 2007 *Acta Phys. Sin.* **56** 2731 (in Chinese)
[16] Ma J, Che C, Yu S Y, Tan L Y, Zhou Y P and Wang J 2012 *Acta Phys. Sin.* 204 (in Chinese)
[17] Fox B P, Simmons-Potter K, Kliner D A V and Moore S W 2013 *J. Non-Cryst. Solids* **378** 79
[18] Mady F, Benabdesselam M, Mebrouk Y and Dussardier B 2010 *Ytterbium-doped Silica Optical Fibers*
[19] Jin J, Li Y, Zhang Z C, Wu C X and Song N F 2016 *Chin. Phys. B* **25** 84213
[20] Gan F and ZhN G Q 1989 *Crystal Color Center Physics* (Shanghai Jiao Tong University Press)
[21] H, D P and Russell P S J 1990 *Opt. Lett.* **15** 102
[22] Song J M, Guo J H, Wang Q X and Hu S L 2012 *Laser & Optoelectronics Prog.* **58–64**